Smart Insole-Based Indoor Localization System for Internet of Things Applications

Diliang Chen, Huiyi Cao, Huan Chen, Zetao Zhu, Xiaoye Qian, Wenyao Xu, *Member, IEEE*, and Ming-Chun Huang, *Member, IEEE*

***Abstract*—With the development of Internet of Things (IoT), indoor localization has been a research focus in recent years. For inertial measurement unit (IMU)-based indoor localization method, zero velocity update (ZUPT) uses the known velocity at stationary epoch as a benchmark to calibrate the velocity drift. However, stationary epoch only takes up 24% of a whole gait cycle time, and the velocity drift at the remaining 76% time is usually estimated according to an assumption that velocity has a linear drift over time, which would introduce errors. In this paper, a two-step velocity calibration method was proposed based on human gait characteristics with Smart Insole: known velocity update (KUPT) and double-foot position calibration (DFPC). KUPT could measure the velocity from heel-strike to toe-off based on the recorded real-time foot angle and the shoe dimensions, which increases the time period when the velocity could be measured from 24% to 62% of a whole gait cycle time. DFPC method could fuse the position information of both feet based on the symmetrical characteristic of human gait to further increase the reliability of the localization results. The statistical result of a 20 times 20-m walking experiment showed that KUPT method was more accurate and reliable than ZUPT method for both feet, and DFPC method could further improve the result of KUPT method. Another experiment about walking in an indoor environment for 91 m showed that the proposed KUPT+DFPC method had an error of about 0.78 m which is acceptable for most IoT applications.**

***Index Terms*—Gait, indoor localization, inertial measurement unit (IMU), Internet of Things (IoT), zero velocity update (ZUPT).**

I. Introduction

With the development of numerous Internet of Things (IoT) enabled applications, accurate real-time localization technologies have attracted much attentions [1]. Thanks to the global positioning system (GPS), outdoor applications could achieve a reliable and accurate localization result if there is no obstacle between the satellites and its receiver [2]. However, in indoor environment, the performance of GPS is not reliable because of factors like multipath effect caused by obstacles, noise, etc. [3]. Indoor localization is important for a diverse range of IoT applications, such as healthcare [4], fitness monitoring [5], pedestrian navigation [6], smart parking [7], etc. In addition, since most people usually spend a considerable amount of time daily (over 80%) indoors to performance various activities, accurate indoor localization technologies became a research focus in recent years [8].

In this paper, a novel two-step indoor localization method was proposed based on human gait: known velocity update (KUPT) and double-foot position calibration (DFPC). According to the normal gait cycle shown in Fig. 1, the human gait consists of stance and swing, which takes about 62% and 38% of the whole gait cycle time, respectively [9]. The stance phase begins with heel-strike, then stationary epoch when the foot was put flat on the ground, and toe-off followed by. For traditionally used zero velocity update (ZUPT) method [10]–[12], only the velocity during stationary epoch is known, which is zero, and the velocity of the remaining 76% gait cycle time has to be estimated. Normally, a widely accepted assumption is that velocity has a linear drift over time [13]–[15]. However, in practice, this method would introduce some errors. KUPT method could decrease the time period when the velocity should be estimated and reduce the introduced errors. Including the stationary epoch, KUPT method could measure the velocity of the whole stance phase based on the dimension of the shoe and the recorded real-time pitch angle. Compared with ZUPT method, KUPT method reduces the time duration when the velocity drift has to be estimated from 76% to 38% of a gait cycle time. In addition, based on the symmetrical characteristics of human gait [16], DFPC was proposed to fuse the stride length of both feet. DFPC method has the potential to increase the localization reliability when the performance of inertial measurement unit (IMU) is not stable over time. The contributions of this paper are as follows.

1) A velocity drift calibration method for IMU-based indoor localization system—KUPT was proposed, which is able to measure the velocity of IMU sensors during gait phases from heel-strike to foot-flat and from heel-lift to toe-off, while ZUPT cannot.
2) DFPC method based on the symmetrical characteristic of human gait was proposed in this paper. This method could fuse the stride length of both feet to help improve the reliability of the final localization result.

Manuscript received February 17, 2019; revised April 16, 2019; accepted May 2, 2019. Date of publication May 9, 2019; date of current version July 31, 2019. This work was funded by the National Science Foundation (NSF-1664368) and by the Ohio Bureau of Workers' Compensation: Ohio Occupational Safety and Health Research Program. *(Corresponding author: Ming-Chun Huang.)*

D. Chen, H. Cao, H. Chen, Z. Zhu, X. Qian, and M.-C. Huang are with the Department of Electrical Engineering and Computer Science, Case Western Reserve University, Cleveland, OH 44106 USA (e-mail: dxc494@case.edu; hhc26@case.edu; hxc556@case.edu; zxz690@case.edu; xxq82@case.edu; mxh602@case.edu).

W. Xu is with the Department of Computer Science and Engineering, State University of New York at Buffalo, Buffalo, NY 14260 USA (e-mail: wenyaoxu@buffalo.edu).

Digital Object Identifier 10.1109/JIOT.2019.2915791

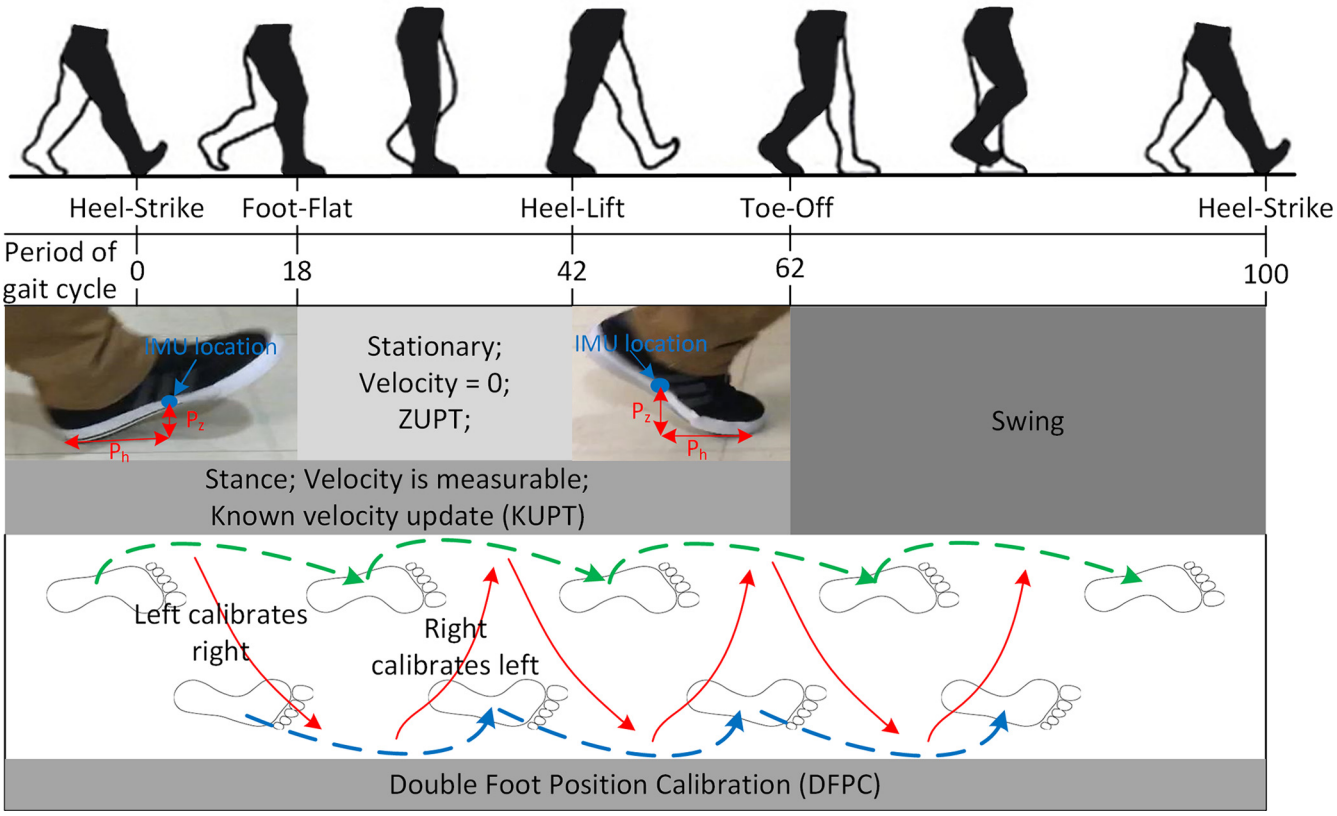

Fig. 1. KUPT+DFPC method based on human gait. KUPT could be applied to the whole "stance" stage (from heel-strike to toe-off) which covered 62% of a gait cycle time. DFPC takes use of the symmetrical characteristics of human gait to calibrate the step distance of one foot with the other foot.

3) The KUPT+DFPC method was embedded into a smartphone application (App) to realize real-time indoor localization.
4) From the experiment results, an interesting finding was discussed that velocity does not drift in a linear way over time.

The rest of this paper is organized as follows. In Section II, the published researches focused on indoor localization and the corresponding limitations are presented. In Section III, details about the Smart Insole system and implementation steps of the proposed KUPT+DFPC method are described. In Section IV, experiments and results are described to show the performance of the proposed indoor localization method. Interesting findings from the experiment results are discussed in Section V. Finally, the paper is concluded and the future works are discussed in Section VI.

II. Related Work

Many technologies have been explored to realize indoor localization, including IMU, acoustic, magnetic, optical, and radio frequency-based technologies [8]. Acoustic-based methods are usually used in limited ranges, and scaling up the coverage area needs higher deployment cost [17], [18]. Magnetic-based method realized localization by using reference stations which generate periodic magnetic field that can by measured by a portable magnetic sensor [19]. However, the application situation of magnetic-based methods is limited by the fact that they are sensitive to conductive and ferromagnetic materials [8]. Optical-based methods like infrared [20], [21], camera [22], laser [23], etc., are limited by high deployment cost and limited coverage area[1]. Radio frequency-based technologies like ultrawideband (UWB) ranging [24], [25], Radio-Frequency Identification (RFID) [26], and radar [27] are affected by multipath propagation problem.

Compared with other indoor localization technologies, IMU-based localization systems have multiple advantages: 1) the cost and size of IMU sensors are reduced significantly in recent decades, which enable inexpensive and straightforward development [28], [29]; 2) they do not need other supporting devices like transmitters, which are necessary for UWB-based localization method, installed and located at the site beforehand. This makes it possible to conduct localization in unknown areas; and 3) suitable for security sensitive scenarios, as IMU does not need to emit any signals during measurement and can remain undetected [28]. These advantages make IMU- based localization systems a research focus in recent years. In terms of where to place IMU sensors, IMU-based localization systems are classified into two categories: 1) waist- and 2) foot-mounted [30]. For waist-mounted systems [31]–[33], since imprecise measurement of acceleration would lead to drift that sums up over time, the position is estimated by multiplying the estimated step lengths and step numbers. Step length is usually estimated based

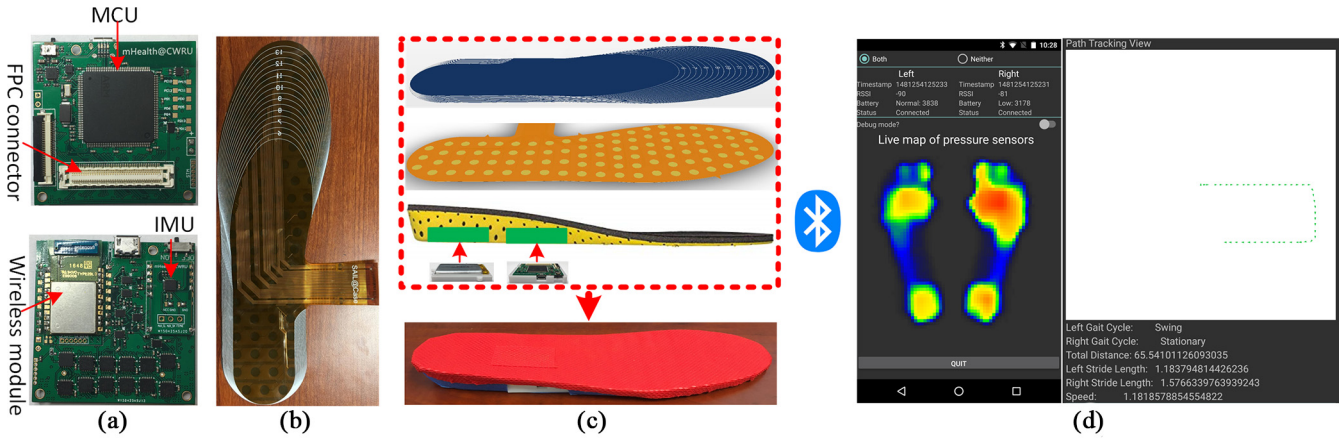

Fig. 2. Smart Insole hardware and the corresponding smartphone App. (a) Details on the circuit board for signal processing and wireless transmission. (b) Insole shaped customizable pressure sensor array. (c) Architecture of the Smart Insole. (d) Smartphone App that works with Smart Insole, which could display real-time information like plantar pressure map, localization results, and gait parameters.

on pedestrian's characteristics, such as weight, height, and age, which is not accurate if the walking pattern is different from the predefined model [34]. It is estimated that the localization error is proportional to the cube of the operation time for inertial navigation systems employing low-cost sensors [35]. To limit the cubic-growth errors, Foxlin [12] proposed to fasten an IMU sensor on shoes. For a normal human gait cycle, there is a time period (i.e., from foot-flat to heel-lift) when the foot would stay stationary and velocity of the IMU attached to the foot is known to be zero. Using the information that velocity of the foot mounted IMU sensor is zero during the stationary epoch of each step to limit the error growth is referred to as ZUPT. To estimate the accumulated errors between two consecutive stationary epochs, the knowledge of when the system has zero velocity is usually used with a model for how the position or velocity errors develop with time [35]. Then the estimated accumulated errors could be used to correct the localization results. ZUPT breaks the cubic-growth localization errors over time and changes it to an error that accumulates linearly with the number of steps. Foot-mounted IMU sensor systems are popularly used for indoor localization research [36]–[38]. However, ZUPT method could only measure the velocity at stationary epoch, and has to estimate the velocity drift in the remaining time period of a gait cycle, which would introduce errors. Many methods have been explored to further reduce the drift after using ZUPT, such as applying Kalman filters [39]–[41] or cooperating with other sensors like UWB sensor [42], barometer [43], RFID [44], [45], etc. Since the drift errors are not always fit the Gaussian distribution, performance of Kalman filters would be decreased [46]. Cooperating with other sensors would make the localization system complex and increase the cost.

All in all, the present indoor localization systems are not suitable for real applications in terms of cost, accuracy, system complexity, etc. To design a low cost, simple, accurate, and real-time indoor localization system, this research further explored the human gait characteristics which cost nothing but could supply important information to help improve the IMU-based localization system.

III. Method

The KUPT+DFPC method makes use of the human gait information to improve the localization accuracy and reliability of IMU-based system. In this section, details on the calibration methods are specified.

A. Hardware System Design

Smart Insole is an important hardware platform used to enable KUPT+DFPC. The hardware of Smart Insole mainly consists a circuit board [Fig. 2(a)] for signal processing and data transmission, and an insole shaped customized pressure sensor array [Fig. 2(b)] for plantar pressure sensing. On the circuit board shown in Fig. 2(a), there is an IMU sensor (accelerometer and gyroscope) for motion sensing, a flexible printed circuit (FPC) connector used to connect the circuit board with the pressure sensor array, a wireless module used to realized data transmission via Bluetooth, and a micro-controller unit (MCU) for controlling the process of data acquisition and transmission. The insole shaped pressure sensor array shown in Fig. 2(b) has 96 pressure sensors equally distributed on it, which make it possible to acquire high resolution plantar pressure data. A customized design method was applied on the pressure sensor array, which makes it possible to fit the requirement on different sizes with one design [47]. The customized design method has been applied in a data glove for hand gesture recognition [48]. For the insole shaped pressure sensor array used in this research, the customized design method makes it possible to fit the foot size from 5.5 U.S. to 14 U.S. with one design. Smart Insole is built by integrating the circuit board and pressure sensor array into an insole shaped package. Fig. 2(c) shows the architecture of the Smart Insole. The top layer is a fabric cover used to ensure the wearing comfort. The insole shaped pressure sensor array is placed on the second layer. The final layer is an insole shaped package which has spaces highlighted with green areas for battery and circuit board. Fig. 2(d) shows a screen shoot of the smartphone App that works with the Smart Insole. Sensor data acquired by Smart Insole could be transferred to the smartphone App via Bluetooth with a data rate of 30 Hz.

The KUPT+DFPC method was realized in the smartphone App which could display the localization result in real-time.

B. Measure the Pressure Noise

Pressure noise is recognized as the pressure value measured during the swing phase when the foot does not apply any pressure on the insole, except the contact pressure noise between the foot and pressure sensors. The pressure noise would influence future data analysis, such as calculating the center of pressure (COP). Therefore, the pressure noise has to be calculated first. To get the pressure noise, a subject would be asked to wear a pairs of Smart Insole and walk normally for 20 s before using the Smart Insole for localization. It is well known that the pressure summation ($P_{\text{total}} = \sum_{k=1}^{96} p_k$) of all the sensors is minimum during the swing phase which takes up 38% of a gait cycle time. Theoretically, to locate the pressure samples corresponding to the swing phase, it is reasonable to find the pressure samples corresponding to the least 38% of the pressure summation. In practice, to avoid the potential disturbances (e.g., the swing phase of a subject does not take up 38% of a gait cycle time because of some kinds of issues or diseases), the percentage of data used for pressure noise calculation could be adjusted accordingly. In this research, the pressure samples corresponding to the least 15% of the pressure summation were used to calculate the pressure noise in case of potential disturbances during experiments. The noise of each pressure sensor could be estimated by (1). For each foot, p^i_{noise} indicates the noise of the ith pressure sensor, n_{swing} indicates the number of samples during the swing phase used for pressure noise estimation, and σ^i_{swing} indicates the standard deviation (STD) of the ith pressure data. Since there are 96 pressure sensors on the pressure sensor array, $i \in [1, 96]$. When doing localization, pressure noise of the raw pressure data could be removed through deleting the corresponding p^i_{noise}

$$p^i_{\text{noise}} = \frac{1}{n_{\text{swing}}} \sum_{k=1}^{n_{\text{swing}}} p^i_k + 3 * \sigma^i_{\text{swing}}. \tag{1}$$

C. Known Velocity Update

As shown in Fig. 1, KUPT method could estimate the velocity during stance phase. Then, only the velocity drift during the remaining swing phase needs to be estimated. To realize KUPT, important gait phases, including heel-strike, stationary, and toe-off have to be recognized first.

1) Stationary Epoch Detection: Some researches used IMU sensors only to find the stationary epoch by comparing the amplitude of the acceleration with a preset threshold. However, noises of the acceleration signal usually make the stationary detection not that accurate. To increase the accuracy of detecting stationary epoch, pressure sensors could be a good choice. Bebek *et al.* [49] used pressure sensors placed under the heel to detect the stationary epoch and achieved a good performance [40]. Different from the pressure sensor array in the research of Bebek *et al.*, which only covers the heel site and mainly used for stationary detection, the pressure sensor array proposed in this research could cover the whole plantar and supply more comprehensive pressure information.

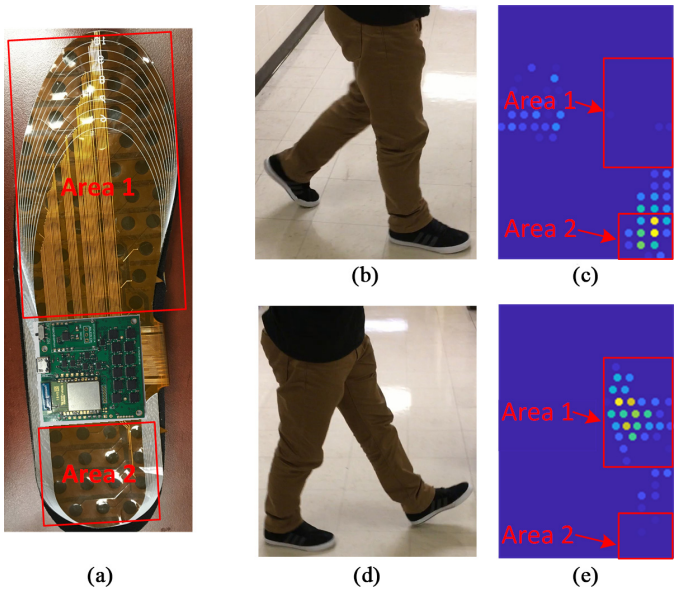

Fig. 3. Stationary epoch detection. (a) Circuit board where the IMU sensor is located separates the pressure sensor array into two areas; (b) and (c) are the posture and the corresponding pressure map when the right foot is at the beginning of the stationary epoch; and (d) and (e) are the posture and the corresponding pressure map when the right foot is at the end of the stationary epoch.

Fig. 3 shows the method used to detect the stationary epoch. To make it easy for method description, the fabric cover [the top layer shown in Fig. 2(c)] was removed from the pressure sensor array and the circuit board [embedded in the third layer shown in Fig. 2(c)] was brought from bottom to top of the pressure sensor array. The relative position in horizontal was not changed. As shown in Fig. 3(a), the pressure sensor array was separated into two areas by the circuit board where the IMU sensor is located. Intuitively, to make the IMU sensor or the circuit board get into stationary epoch during a normal gait cycle, there must be some forces applied to both the upper and lower side the circuit board. In other words, when there are forces applied to both area 1 and area 2 of the pressure sensor array during a normal human gait, the IMU sensor should be in stationary epoch. To confirm this deduction, an experiment was done by asking a subject to walk normally with Smart Insole for several steps, during which the walking gait was recorded by a camera. Timestamps of the camera and Smart Insole were recorded at the same time for data synchronization. Stationary epoch of a step could be recognized manually from the recorded video frames, then the pressure map corresponding to the stationary epoch could be located. Fig. 3(b) shows the posture when right foot is at the beginning of the stationary epoch, and Fig. 3(c) shows the corresponding plantar pressure map. It could be seen that although most pressure is concentrated on area 2, three pressure sensors on area 1 are starting to be activated. Fig. 3(d) and (e) shows the posture and the corresponding plantar pressure when right foot is at the end of the stationary epoch. It could be seen that most pressure is concentrated on area 1, but two pressure sensors on area 2 are still in active.

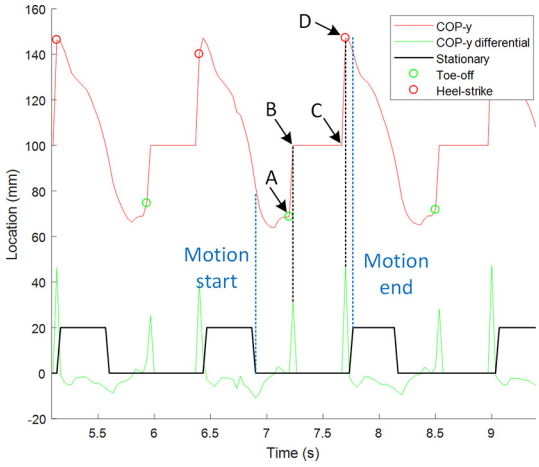

Fig. 4. Detection method for toe-off and heel-strike event. Point B and C indicate the first and last sample of the swing epoch. Point A and D indicate the detected toe-off and heel-strike event. High and low level of the black line indicates the stationary and nonstationary epoch, respectively.

2) Heel-Strike and Toe-Off Detection: Heel-strike and toe-off were detected from COP signal. Horizontal and vertical coordinators of COP were calculated with the following equations:

$$\text{copX} = \frac{\sum_{i=1}^{n} x_i p_i}{\sum_{i=1}^{n} p_i} \tag{2}$$

$$\text{copY} = \frac{\sum_{i=1}^{n} y_i p_i}{\sum_{i=1}^{n} p_i} \tag{3}$$

where copX and copY refer to the horizontal and vertical coordinates of COP, respectively; n refers to the number of pressure sensors on each insole; x and y refer to the horizontal and vertical coordinates of a sensor; and p refers to the pressure value of a measured sensor. COP was calculated for both feet.

According to (2) and (3), COP is a 2-D signal. In the direction from toe to heel, the y-axis of COP could be increased from 34 mm (the least coordinate of the sensor on the toe area) to 166 mm (the largest coordinate of the sensor on the heel area) for the Smart Insole used in this research. Since it is less likely for a foot to touch sensors with the least or largest coordinate without touching other adjacent sensors, the y-axis of COP usually cannot reach 34 mm or 166 mm. As shown in Fig. 4, the calculated y-axis of COP (COP-y) ranges from about 70 to 150 mm in the experiment. During the swing epoch, since there was no pressure applied on the pressure sensor array, COP was set to the foot center which is 100 mm in the y-axis. As shown in Fig. 4, the time period when the COP-y is kept to 100 mm indicates the swing epoch of each step. In Fig. 4, point B and C indicate the first and last sample of the swing epoch. During the gait cycle, y-axis of COP would be increased significantly from 100 mm to about 150 mm when gait event was transferred from swing (point C) to heel-strike (point D), and be increased significantly from about 70 to 100 mm when the gait event was transferred from toe-off (point A) to swing (point B). Based on this fact, heel-strike could be located by finding the maximum of COP differential signal in the time period from swing to motion end (i.e., foot-flat or the first sample of the stationary epoch), and toe-off could be located by finding the maximum of COP differential signal from motion start (i.e., heel-lift or the first sample of the nonstationary epoch) to swing. For example, as shown in Fig. 4, in the time period from swing (point C) to motion end (the blue dashed line on the right), the maximum of COP differential signal (the black dashed line on the right) occurred when COP-y changed from point C to point D, so point D is recognized as heel-strike. Similarly, in the time period from motion start (the blue dashed line on the left) to swing (point B), the maximum of COP differential signal (the black dashed line on the left) occurred when COP-y changed from point A to point B, so point A is recognized as toe-off.

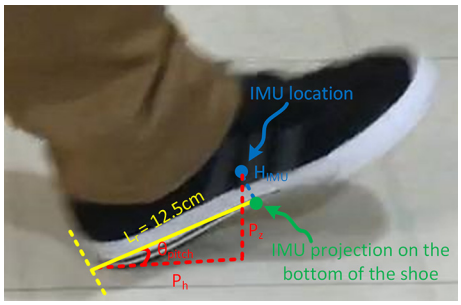

Fig. 5. Calculate the IMU location from heel-strike to motion end. The blue dot indicates the location of IMU and the green dot indicates the IMU projection on the bottom of the shoe, H_{imu} indicates the distance between IMU and its projection, θ_{pitch} indicates the rotation angles of the IMU, L_r indicates the rotation radius of the IMU projection. P_z indicates the vertical location of the IMU and P_h indicates the horizontal distance between the IMU and heel.

3) Implementation of KUPT: KUPT uses the known velocity of an IMU sensor to calibrate the velocity calculated from the raw IMU signals (e.g., acceleration and gyroscope signal). The IMU sensor is packed inside an insole shaped package, as shown in Fig. 2(c). In practice, the Smart Insole would be placed inside a shoe just as the use of a regular insole. Fig. 5 shows the IMU location tracking method from heel-strke to motion end with a side view diagram. The blue dot shows the IMU location from a side view. The green dot indicates the IMU projection on the bottom of the shoe. When customized the pressure sensor array to 10.5 U.S. size and placed it into a 10.5 U.S. size shoe, the distance from the green dot to the heel is 12.5 cm. Since the sole around heel area is the most rigid and usually does not have shape change during normal walking, the rotation radius (L_r) of the green dot is 12.5 cm from heel-strike to motion end. H_{imu} is the distance from IMU to its projection on the bottom of the shoe, including the thickness of the shoe sole and the distance from IMU to the bottom of Smart Insole, which is 2.9 cm in this experiment. θ_{pitch} could be acquired from IMU sensor directly in real-time. Therefore, from heel-strike to motion end, the location of IMU sensor could be acquired according to the following equations:

$$\begin{cases} P_h = L_r * \cos(\theta_{\text{pitch}}) - H_{\text{imu}} * \sin(\theta_{\text{pitch}}) \\ P_x = P_h * \cos(\theta_{\text{yaw}}) \\ P_y = P_h * \sin(\theta_{\text{yaw}}) \\ P_z = L_r * \sin(\theta_{\text{pitch}}) + H_{\text{imu}} * \cos(\theta_{\text{pitch}}) \end{cases} \tag{4}$$

where L_r indicates the distance between heel end and the IMU projection on the bottom of the shoe, which is 12.5 cm for

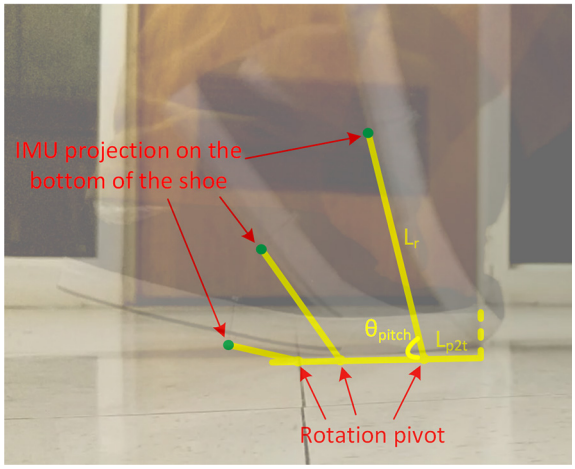

Fig. 6. Location changes of the IMU projection on the bottom of the shoe from motion start to toe-off. Three instant postures of a foot were selected to show the location change over time. The green dots indicate the IMU projection on the bottom of the shoe. The yellow dots indicate the rotation pivot of the IMU projection, θ_{pitch} indicates the rotation angle of the IMU, L_r indicates the rotation radius of the IMU projection, and L_{p2t} indicates the distance between the rotation pivot and the toe.

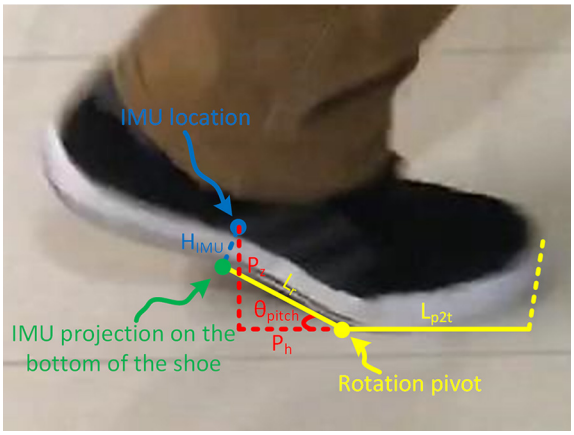

Fig. 7. Calculate the IMU location from motion start to toe-off. The blue dot indicates the location of IMU. The green dot indicates the IMU projection on the bottom of the shoe. H_{imu} indicates the distance between IMU and its projection. The yellow dot indicates the rotation pivot of the IMU projection. θ_{pitch} indicates the rotation angle of the IMU. L_r indicates the rotation radius of the IMU projection, and L_{p2t} indicates the distance between the rotation pivot and the toe. P_z indicates the vertical location of the IMU and P_h indicates the horizontal distance between the IMU and rotation pivot.

the 10.5 U.S. shoe used in this research; H_{imu} indicates the distance between the IMU and its projection on the bottom of the shoe. θ_{pitch} and θ_{yaw} indicate the rotation angels in vertical and horizontal axes, respectively

$$\begin{cases} V_k^x = \left(P_{k+1}^x - P_k^x\right)/T_s \\ V_k^y = \left(P_{k+1}^y - P_k^y\right)/T_s \\ V_k^z = \left(P_{k+1}^z - P_k^z\right)/T_s \end{cases} \tag{5}$$

where V_k^z indicates the vertical velocity at the kth sample; P_k^z indicates the vertical distance at the kth sample; and T_s indicates the sample period.

From motion start to toe-off, the IMU sensor is rotated around a curve with varying radius. Fig. 6 uses three instant postures of a foot to show the location change of the IMU projection on the bottom of the shoe from motion start to toe-off. The distance between green dot (i.e., IMU projection on the bottom of the shoe) and the corresponding yellow dot (i.e., rotation pivot) is the rotation radius (L_r). It is obvious that the rotation radius is not constant from motion start to toe-off. Fig. 7 shows an IMU location calculation method from motion start to toe-off with a side view diagram. H_{imu} could be measured directly, which is 2.9 cm for the shoe used in the experiment. θ_{pitch} is the rotation angle of the IMU that could be measured by the IMU in real time. In order to calculate the vertical location (P_z) and the horizontal location corresponding to the toe ($P_h + L_{\text{p2t}}$), rotation radius of the IMU projection (L_r), and the distance between rotation pivot and the toe (L_{p2t}) are necessary. From Fig. 6, it is obvious that L_r and L_{p2t} are related to θ_{pitch} for normal walking. In this research, a curve fitting method was used to get the relation between θ_{pitch} and L_r and L_{p2t}. Since there are low variabilities in a normal human gait [50], the curve fitting method could have an acceptable prediction accuracy. To get the data for curve fitting, the subject performed five different static postures, which were transit postures in the dynamic motion from motion start to toe-off, with different θ_{pitch} for three times. During the experiment, L_r, L_{p2t} were measured with rulers, and the corresponding θ_{pitch} of each posture was recorded by the smartphone App.

When doing localization, the fitting curve was used to predict L_r and L_{p2t} based on the real-time θ_{pitch}. With L_r, L_{p2t}, and the measurable parameters H_{imu}, θ_{pitch}, and θ_{yaw}, position and velocity could be calculated according to the following equations:

$$\begin{cases} P_h = L_r * \cos\left(\theta_{\text{pitch}}\right) - H_{\text{imu}} * \sin\left(\theta_{\text{pitch}}\right) \\ P_x = \left(P_h + L_{\text{p2t}}\right) * \cos\left(\theta_{\text{yaw}}\right) \\ P_y = \left(P_h + L_{\text{p2t}}\right) * \sin\left(\theta_{\text{yaw}}\right) \\ P_z = L_r * \sin\left(\theta_{\text{pitch}}\right) + H_{\text{imu}} * \cos\left(\theta_{\text{pitch}}\right) \end{cases} \tag{6}$$

$$\begin{cases} V_k^x = -\left(P_{k+1}^x - P_k^x\right)/T_s \\ V_k^y = -\left(P_{k+1}^y - P_k^y\right)/T_s \\ V_k^z = \left(P_{k+1}^z - P_k^z\right)/T_s \end{cases} \tag{7}$$

where V_k^z indicates the vertical velocity at the kth sample; P_k^z indicates the vertical distance at the kth sample; and T_s indicates the sample period.

In general, velocity drift is estimated according to an assumption that velocity has a linear drift over time. Although velocity does not drift strictly linear over time in practice, the estimation could give reasonable result if the applied time duration is short. Compared with ZUPT method, KUPT method significantly decreased the time duration when velocity drift has to be estimated, which helps KUPT get better result. During swing epoch, velocity drift could be estimated according to the following equation:

$$\begin{cases} V_{\text{errt}} = V_{\text{kt}}^{\text{raw}} - V_{\text{kt}}^{\text{ref}} \\ V_{\text{errh}} = V_{\text{kh}}^{\text{raw}} - V_{\text{kh}}^{\text{ref}} \\ \text{driftrate} = (V_{\text{errh}} - V_{\text{errt}})/(\text{kh} - \text{kt}) \\ V_k^{\text{calibrated}} = V_k^{\text{raw}} - V_{\text{errt}} - \text{driftrate} * (k - \text{kt}) \\ (k \in [\text{kt} + 1, \text{kh}]) \end{cases} \tag{8}$$

where V_{errt} and V_{errh} (shown in Fig. 8) indicate the velocity error at the toe-off and heel-strike event of the same gait cycle,

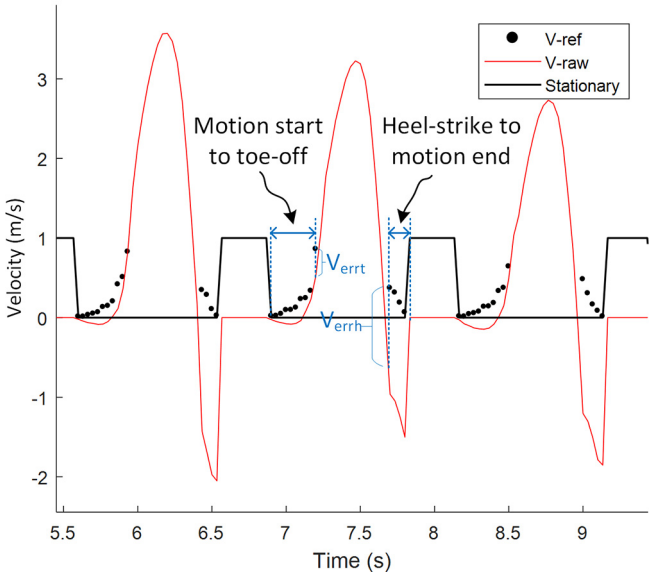

Fig. 8. Demonstration of velocity calibration. The black line indicates the stationary state of the IMU. High level indicates stationary epoch, and low level indicates nonstationary epoch. The red line indicates the velocity calculated from the raw acceleration, and its value was forced to zero when the IMU was in stationary state. Black dots indicate the reference velocity calculated from the measured position of the IMU.

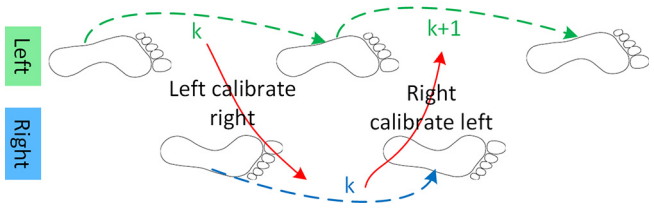

Fig. 9. Demonstration of DFPC implementation. Green dashed lines indicate the walking direction of the left foot and the blue dashed line indicates the walking direction of the right foot. Red lines indicate the calibration direction.

respectively. kt and kh indicate the index number for the data corresponding to the toe-off and heel-strike event. Therefore, $V_{\text{kt}}^{\text{raw}}$ and $V_{\text{kh}}^{\text{raw}}$ indicate the raw velocity at toe-off and heel-strike event, respectively. driftrate indicates the velocity drift rate between toe-off and heel-strike event (i.e., swing epoch). $V_k^{\text{calibrated}}$ indicates the calibrated kth velocity data between toe-off and heel-strike.

4) Double-Foot Position Calibration: DFPC takes use of the symmetrical characteristic of a normal human gait to fuse the position information from both feet. Fig. 9 shows the way to do DFPC when left foot walked first. The kth step of the left foot was used to calibrate the stride length of the kth right foot step, and the kth right foot step was used to calibrate the $(k+1)$th foot step of the left foot. Calibration coefficient is a parameter used to determine how to fuse the stride length calculated from both feet, which consists two factors: 1) one is the correlation r between two corresponding steps and 2) the other is the error index (EI) of each foot.

Correlation between two corresponding steps was introduced as a measure of the similarity of these two steps. During normal walking, activities of both feet are symmetry in most of the time, but there are indeed sometimes when the walking activities are different. For example, when a subject is changing the walking speed, then walking pattern of the adjacent step of both feet would be different. At this time, the walking distance of one foot is not suitable to calibrate the other foot. To make the calibration coefficient automatically adjust its value to reflect the similarity of the corresponding two steps, the correlation parameter r is necessary. Activity changes could be reflected on the changes of plantar pressure, based on which working activities could be recognized in our former researches [51], [52]. During walking activities, the whole human body is supported by foot. Therefore, the changes of walking activities will be reflected on the changes of plantar pressure, then reflect on the changes of COP over time, especially the COP along the line from heel to toe. Therefore, copY signal was used to calculate the correlation between the corresponding steps

$$r = \left| \frac{\sum_{i=1}^{n}(x_i - \bar{x}) * (y_i - \bar{y})}{\sqrt{\sum_{i=1}^{n}(x_i - \bar{x})^2} * \sqrt{\sum_{i=1}^{n}(y_i - \bar{y})^2}} \right| \tag{9}$$

where, n is the number of samples of a step; x_i and y_i indicate the ith copY of each foot, respectively; and $\bar{x} = (1/n) * \sum_{i=1}^{n} x_i, \bar{y} = (1/n) * \sum_{i=1}^{n} y_i$.

EI is the velocity error at heel-strike and toe-off event, which is used as a measure of the velocity drift introduced by the acquired IMU signal. Lower EI indicates that there is less drift in the acquired IMU signal, then the estimated location is expected to have a higher accuracy, vice versa. EI of each foot was calculated as the absolute of the sum of the differences between raw velocity and reference velocity at heel-strike and toe-off event, respectively

$$\text{EI} = |V_{\text{errt}} + V_{\text{errh}}|. \tag{10}$$

Calibration coefficient is calculated according to the following equations:

$$\begin{cases} \text{Calicoef}_L = \frac{\text{EI}_R/r_L}{(\text{EI}_R/r_L + \text{EI}_L)} \\ \text{Calicoef}_R = \frac{\text{EI}_L/r_R}{(\text{EI}_L/r_R + \text{EI}_R)}. \end{cases} \tag{11}$$

Take Fig. 9 for example, the $(k+1)$th stride length of left foot is calibrated with the kth right stride length according to the following equation:

$$D_{k+1}^{L} = d_{k+1}^{L} * \text{Calicoef}_L + d_k^R * (1 - \text{Calicoef}_L) \tag{12}$$

where, D_{k+1}^{L} indicates the calibrated stride length of the $(k+1)$th left step, d_{k+1}^{L} indicates the stride length of the $(k+1)$th left step calculated with KUPT, and d_k^R indicates the stride length of the kth right step calculated with KUPT.

Through (11) and (12), the calibrated stride length could reflect the influence of EI and similarity of the corresponding two steps. For example, as shown in Fig. 9, if the $(k+1)$th left step is similar with the kth right step, that is, $r_L \approx 1$, but EI_L is higher than EI_R, then Calicoef_L would be lower than 0.5, that is, the calibrated $(k+1)$th left stride length (D_{k+1}^{L}) would put more weight on the kth right stride length (d_k^R). On the other hand, if EI_L is similar with EI_R, but the similarity between the $(k+1)$th left step and the kth right step is low (e.g., $r_L \approx 0$),

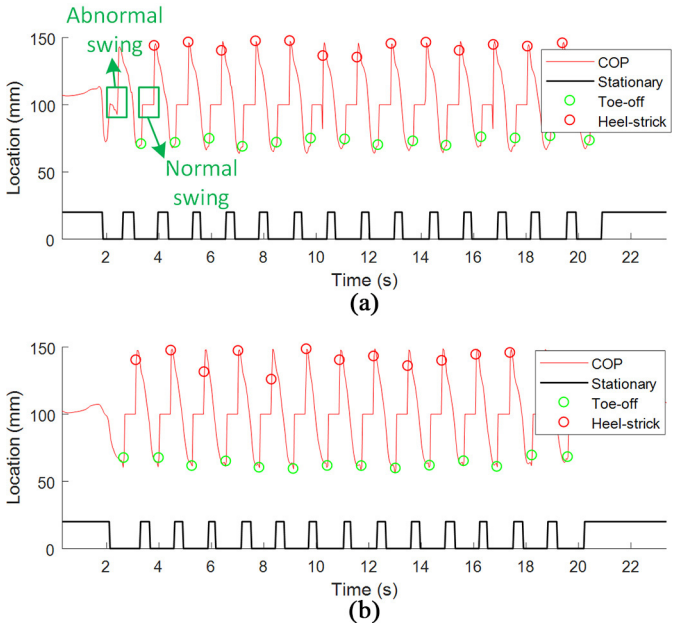

Fig. 10. COP of left (a) and right (b) foot. Red circles indicate the detected heel-strike event. Green circles indicate the detected toe-off event. The high level of black line indicates the stationary epoch.

then Calicoef$_L \approx 1$, that is the calibrated $(k+1)$th left stride length (D^L_{k+1}) would put more weight on the $(k+1)$th left stride length (d^R_{k+1}).

At this point, two calibrated localization results were acquired from both feet. To decide which result to use, a distance weighted error was introduced

$$\sum_{k=1}^{n}(\mathrm{EI}^L_k - \mathrm{EI}^R_k) * \frac{|D^L_k| + |D^R_k|}{2} \tag{13}$$

where, n is the number of steps before applying (13); EI^L_k and EI^R_k indicate the kth EI of left and right foot, respectively; D^L_k and D^R_k indicate the kth calibrated stride length of left and right foot, respectively. When the above equation is positive, which means the distance weighted error of left foot is higher, then the calibrate path based on right foot will be used, vice versa.

IV. Experiments and Results

In this section, the experiments and results were described to show the performance of gait event detection and the advantage of KUPT+DFPC in comparison with the popularly used ZUPT method.

A. Performance of Gait Event Detection

Detection of gait events, such as stationary, heel-strike, and toe-off is important for the application of KUPT+DFPC. To show the performance of gait events detection, an experiment was done by a subject walking normally for a distance of 20 m. During the experiment, the subject was wearing a pair of Smart Insole with a size of 10.5 U.S. Fig. 10(a) and (b) shows the detected toe-off (green circles), heel-strike (red circles), and stationary epoch (high level of the black lines) of the left and right foot, respectively. As shown in Fig. 10, toe-off, heel-strike, and stationary epoch could be detected correctly. Toe-off and heel-strike of the first left step were not extracted, because that step was recognized as abnormal. During a normal swing phase, the COP should stay at a location (its 100 for this experiment setup) for a while, as shown in Fig. 10. It is obvious that the first left step does not have a normal swing which makes that step recognized as abnormal. Therefore, toe-off and heel-strike were not extracted for that step to do position calibration.

B. Accuracy and Reliability of KUPT+DFPC

In this section, experiments were designed to evaluate the accuracy and reliability of the proposed KUPT+DFPC method, and a comparison was made with the popularly used ZUPT method. During the experiment, a subject wearing a pair of 10.5 U.S. sized Smart Insole walked in his comfort walking speed for a distance of 20 m for 20 times. The walking distance of 20 m was selected, because the advantage of KUPT+DFPC over ZUPT could be accumulated step by step. The walking distance of 20 m usually has 15 steps for the subject involved in the experiment. The accumulated difference of these steps could be enough to show the difference between KUPT+DFPC and ZUPT. The experiment data on one 20 m walking session was used to show the detailed result of each step of KUPT+DFPC method. The statistical results of 20 times walking were used to show the accuracy and reliability of the proposed method [1].

1) Detailed Result of Each Step of KUPT+DFPC: As discussed in Section III, the method of KUPT+DFPC could be separated into three steps: a) implementing KUPT method to get the calibrated velocity, then walking distance; b) calibrating the walking distance of one foot with the other foot, which is called the 1st stage DFPC; and c) finishing the DFPC method by using (13) to make a decision on which of the two calibrated walking distances with the 1st stage DFPC will be used as an output. In the following, an insight and intuitive view of the result of each step of KUPT+DFPC would be shown. In addition, the result of ZUPT method was used as a comparison.

Fig. 11 shows the results of all the important steps of KUPT+DFPC. Fig. 11(a) and (b) shows the velocity acquired from the left and right foot, respectively. To show the plot details more clearly, the velocity plot in the dashed box was zoomed in. The black line indicates the stationary status, and high level of the black line indicates the time period when the IMU was in stationary epoch. Green lines indicate the raw velocity (V-raw) that was directly calculated from the IMU signal. To make it easy to see the velocity drift of each step in V-raw, V-raw was forced to zero during the stationary epoch to limit the accumulation of velocity drift across steps. Black dots indicate the reference velocity (V-ref) which was calculated based on the measured location of IMU from motion start to toe-off and from heel-strike to motion end. The differences between V-raw and V-ref were the velocity drift. It is obvious that V-raw of many steps, including the zoomed in step, has a lot velocity drift. The blue and red line indicate

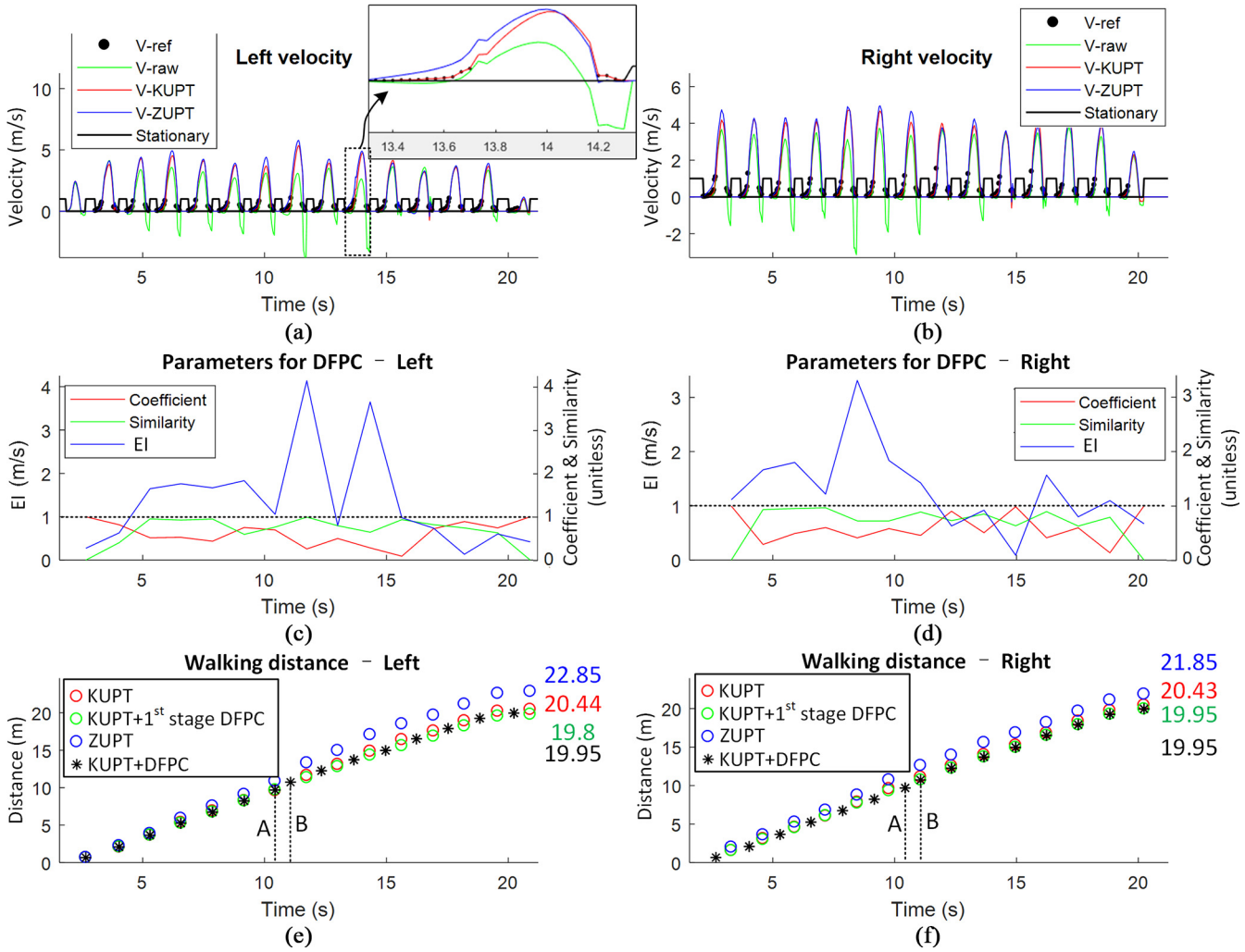

Fig. 11. Detailed results of each step of KUPT+DFPC. (a) and (b) show the detected stationary epoch and the velocity calculated with different methods. (c) and (d) show the parameters necessary for DFPC. (e) and (f) show the walking distance calculated with ZUPT, KUPT, KUPT+1st stage DFPC, and KUPT+ZUPT method.

the velocity calculated with ZUPT and KUPT, respectively. Although velocity drift could be decreased by ZUPT, there was still some drift from V-ref. By taking use of V-ref, KUPT could get a better performance than ZUPT on velocity calibration. Through integrating the velocity over the corresponding step time, stride length could be calculated. Walking distance could be acquired by accumulating the stride length step by step. As shown in Fig. 11(e) and (f), red and blue circles indicate the accumulated walking distance after each stride based on KUPT and ZUPT method, respectively. For example, the first red circle indicates the walking distance of the first stride based on KUPT, and the second red circle indicates the accumulated walking distance of the first and second stride based on KUPT, and so on.

In the following, the stride length calculated based on KUPT method would be further processed by the 1st stage DFPC, during which the stride length of one foot would be calibrated with the latest stride length of the other foot. In this process, parameters involved, including "similarity," "EI," and "coefficient." As shown in (12), coefficient determines how to fuse the stride length of both feet. Similarity and EI could adaptively change coefficient via (11), then influence the fusion results. As shown in Fig. 11(c) and (d), the green line indicates the similarity of the sequentially left and right steps. Except for the first and last steps, the sequentially left and right foot steps are with high similarity (similarity values are close to "1"). This result indicates that fusing the stride length of the left and right foot is reasonable. For the left foot, low similarity of the first step is caused by the fact that the left foot took the first step in the experiment, so there was no right step that could be used for calibration. Similarity of the first right step is low, because the first left step could be seen as a half stride, while the first right step was a full stride, thus the significant difference between these two steps leads to the low similarity. The low similarity of the last step of both the left and right foot was caused by the fact that the subject needed to adjust the last stride length to make both feet stepped on the finishing line which indicates the end of the 20-m experiment. The adjustment on stride length led to the change of walking pattern and then caused a low similarity. The blue line indicates EI. It is obvious that changes of EI are corresponding to the velocity drift of V-raw. The red line indicates coefficient,

TABLE I
STATISTICAL RESULTS

	ZUPT-L	ZUPT-R	KUPT-L	KUPT-R	KUPT+DFPC
Mean (m)	20.97	21.16	19.58	20.44	20.08
STD (m)	1.84	0.73	1.24	0.5	0.51
Q1 (m)	19.74	20.61	18.67	20.14	19.74
Median (m)	21.17	21.07	19.64	20.36	20.06
Q3 (m)	22.56	21.62	20.77	20.52	20.46

changes of which is adaptive to the corresponding similarity and the EI of both feet. Through coefficient, stride length of both feet could be calibrated with the 1st stage DFPC. Green circles shown in Fig. 11(e) and (f) indicate the accumulated walking distance after each stride based on KUPT+1st stage DFPC.

Finally, (13) was used to finish DFPC and make a decision on which of the two calibrated walking distances with the 1st stage DFPC would be used as an output. Equation (13) evaluated the summation of the stride length weighted EI of all the past steps. If the summation of left foot was higher than right foot, which indicated that the IMU of left foot introduced more drift, then the output of (13) would be positive and the walking distance of right foot would be used as an output. Since (13) was applied after every step, the decision on using the walking distance of which foot could also be adaptively changed after every step. As shown in Fig. 11(e) and (f), black stars indicate the finalized walking distance after each step. From the beginning to time A, it is obvious that each black star is located at the same location as a green circle in Fig. 11(e), but not (f), which indicates that the walking distance of the left foot is selected in this time period. This result could be explained by comparing the EI of both feet shown in Fig. 11(c) and (d). It is obvious that summation of the stride length weighted EI for steps before time A are lower for left foot. From time B to the end, two significantly high peaks in left EI make (13) positive for all the steps in this time period, and the walking distance of right foot was selected. This result indicates that the drift of IMUs could change significantly over time, and it is necessary to fuse the data of both feet and select a better result dynamically.

Colored numbers shown in Fig. 11(e) and (f) indicate the walking distance calculated with different methods. It is obvious that the walking distances calculated based on KUPT (red colored numbers, left: 20.44 m, right: 20.43 m) were more closed to the ground truth (i.e., 20 m) than ZUPT (blue colored numbers, left: 22.85 m, right 21.85 m), and the fused walking distances with KUPT+1st stage DFPC (green colored numbers, left: 19.8 m, right: 19.95 m) got even better results for both left and right foot. Finally, a better result (black colored numbers, left and right: 19.95 m) was correctly chosen to represent the walking distance.

2) Statistical Results of KUPT+DFPC: Table I shows mean, STD, first quartile (Q1), median, and third quartile (Q3) of the estimated distances acquired from all the 20 experiments with ZUPT, KUPT, and KUPT+DFPC methods, respectively. For the distance estimated by ZUPT and KUPT methods, the statistical results of both feet were displayed. For KUPT+DFPC, only the final localization result

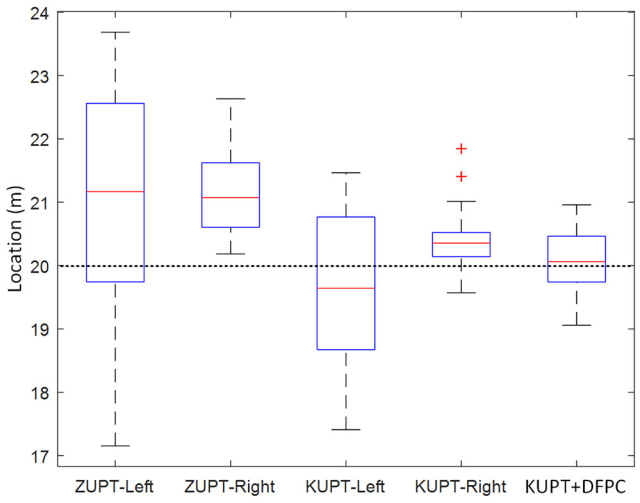

Fig. 12. Box plot of the estimated distances from all the 20 experiments based on ZUPT, KUPT, and KUPT+DFPC, respectively.

of each experiment was used for statistical analysis. Fig. 12 used box plot to show the statistical results more intuitively. From Fig. 12 and Table I, it is obvious that the mean value of KUPT method (left: 19.68 m, right: 20.44 m) is more closed to ground truth (20 m) compared to the ZUPT method (left: 20.97 m, right: 21.16 m) for both feet. By comparing the median results, KUPT method also has a better performance. The KUPT method (left: 1.24 m, right: 0.5 m) also has smaller STD when compared with ZUPT method (left: 1.84 m, right: 0.73 m). In addition, KUPT+DFPC further improved the localization accuracy in terms of "mean" and "median." Therefore, statistical results indicate that KUPT method has a better performance than ZUPT method, and DFPC method also helps improve the KUPT performance.

From Fig. 12 and Table I, two other observations could be acquired.

1) The accuracy of localization results of the left and right foot are similar in terms of mean and median for both ZUPT and KUPT methods, which indicates that similar localization accuracy could be expected from the left and right foot. For ZUPT method, the mean value of localization results for the left and right foot are 20.97 and 21.16 m, respectively. Since the actual distance is 20 m, the accuracy is $|20.97-20|/20 = 4.9\%$, and $|21.16-20|/20 = 5.8\%$. Similarly, the accuracy in term of median value is 5.85% and 5.35% for the left and right foot, respectively. For KUPT method, the accuracy in terms of mean value is 2.1% and 2.2% for the left and right foot, and the accuracy in terms of median is 1.8% and 1.8%, for the left and right foot, respectively.
2) Localization results of the left foot are distributed in a larger range than the right foot for both ZUPT and KUPT method. This might be caused by two reasons: a) performance differences between the IMU on the left and right foot. Although the IMU sensors used on the left and right foot could acquire similar accuracy in terms of mean and median value, there might be some differences on the performance of stability which could lead to some

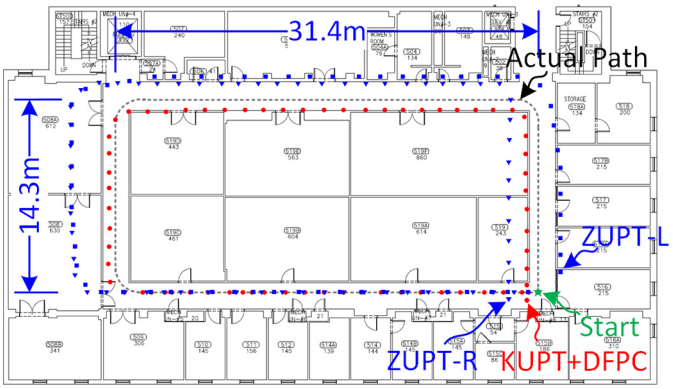

Fig. 13. Performance of the proposed KUPT+DFPC method in practice. Red dots, blue squares, and blue triangles indicate the position of each step calculated with KUPT+DFPC, ZUPT of the left foot, and ZUPT of the right foot, respectively. The gray dashed line indicates the actual path of the experiment. The green star indicates the start position. The end positions of the path calculated with KUPT+DFPC, ZUPT of the left foot, and ZUPT of the right foot were marked with texts "KUPT+DFPC," "ZUPT-L," and "ZUPT-R," respectively.

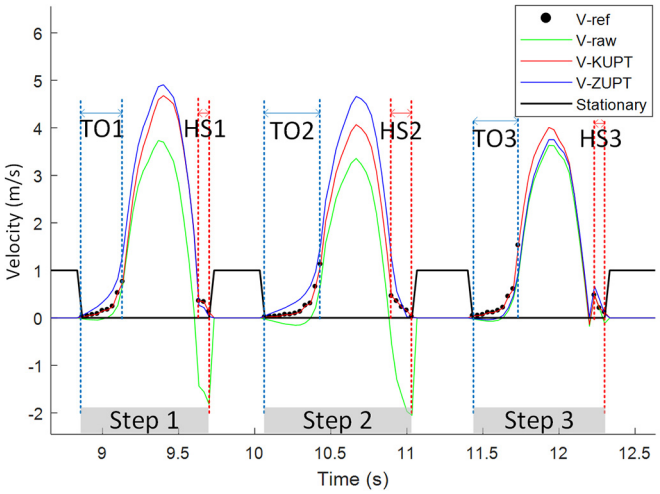

Fig. 14. Characteristics of velocity drift. "TO" is an abbreviation of toe-off and "HS" is an abbreviation of heel-strike.

differences on deviation of the localization results and b) gait patterns of the left and right foot are not the same exactly. Although high symmetry could be observed between the left and right foot in a normal walking gait, they are not exactly the same. This thought is confirmed by the similarity results shown in Fig. 11(c) and (d). The similarity results are closed to 1 in Fig. 11(c) and (d) indicates that the gait of left and right foot is with high symmetry. However, since the similarity results are not equal to 1, there might be some kinds of differences between the gait of left and right foot, which could influence the performance of IMU sensors, then lead to the difference of result distribution.

C. Performance of KUPT+DFPC in Practice

To test the performance of the proposed KUPT+DFPC method in practice, an experiment involved the activity of walking around in a building was designed. During the experiment, a subject was wearing a pair of Smart Insole with a size of 10.5 U.S., and walked normally around the 5th floor of Glennan Building. Fig. 13 shows the position of each step calculated with KUPT+DFPC (red dots), ZUPT of the left foot (blue squares), and ZUPT of the right foot (blue triangles). Compared with the paths calculated with ZUPT of the left and right foot, the path calculated with KUPT+DFPC has less drift from the actual path (gray dashed line). In terms of the total walking distances, the drifts introduced by ZUPT of the left foot, ZUPT of the right foot, and KUPT+DFPC were 11.15, 7.43, and 0.78 m, respectively. Total distance of the actual path is around 91 m. Therefore, the error introduced by KUPT+DFPC is around 0.86% which is acceptable for most indoor localization applications.

V. Discussion

Experiment results showed the accuracy and reliability of the proposed two-step indoor localization method: KUPT+DFPC. In addition, an interesting finding about the characteristics of the velocity drift was found from the experiment results. As mentioned in the section—"KUPT," KUPT method which could estimate the velocity of an IMU from "motion start" to "toe-off," from "heel-strike" to "motion end" and in stationary epoch. Compared with traditional ZUPT method, the time duration when the IMU velocity could be measured was extended from 24% to 62% of a gait cycle time. And this extended time duration makes it possible to get more insight about the characteristics of velocity drift. For the time duration when the velocity cannot be measured, velocity drift is estimated according to a widely accepted assumption that velocity has a linear drift over time [13]–[15]. However, the experiment results did not support this assumption. As shown in Fig. 14, 4 different kinds of velocity of three continuous steps were displayed. "TO1," "TO2," and "TO3" indicate the time period from motion start to toe-off of the corresponding steps, which are highlighted with two dashed blue lines. "HS1," "HS2," and "HS3" indicate the time period from heel-strike to motion end of the corresponding steps, which are highlighted with two dashed red lines. Through comparing the "V-ref" and "V-raw" in the time period indicated with TO1, TO2, and TO3, it is obvious that the velocity difference (i.e., velocity drift) is not changed linearly with time. In TO1 and TO2, the velocity difference is increased at first and then decreased. While in TO3, the velocity difference is increased at first, then decreased, and finally increase again.

Velocity drift could be introduced during a short period of time which could occur at any gait phase. At the end of step 1, the velocity bias between V-ref and V-raw is -1.818 m/s. Although the velocity between V-ref and V-raw is not the same all the way during TO1, both V-ref and V-raw changed from 0 to 0.76 m/s at the end of TO1. Therefore, there is no velocity drift introduced during TO1. Similarly, the velocity change of V-ref and V-raw during HS1 is almost the same, so there is almost no velocity drift introduced during HS1. Therefore, most of the velocity drift of step 1 is introduced during the swing phase. For step 2, the velocity drift is -2.05 m/s

which is mainly introduced in HS2. During HS2, V-ref was changed from 0.46 to 0, and V-raw was changed from −0.55 to −2.05 m/s, so the velocity drift introduced was −1.04 m/s. Similarity, the velocity drifts introduced during TO2 and the swing phase were −0.42 and −0.59 m/s. Through comparing the velocity drift of all these three steps, it is obvious that velocity drift could be significantly different between steps. The velocity drift of steps 1 and 2 were around −2 m/s, while the velocity drift of step 3 was −0.12 m/s.

Although the assumption that velocity has a linear drift over time does not reflect the real situation, it could still be a reasonable assumption if the time duration to adopt this assumption is short. Therefore, the KUPT method proposed in this research is necessary to decrease the error introduced by the assumption, because KUPT could significantly decrease the time duration, during which the velocity is not measurable, from 76% to 38% of the whole gait cycle time.

VI. Conclusion

In this paper, a two-step IMU-based indoor localization method was proposed—KUPT+DFPC. Compared with ZUPT method, KUPT extended the time period when the velocity could be measured from 24% to 62% of a gait cycle time, which is helpful to reduce the velocity drift estimation errors. DFPC takes use of the symmetrical characteristics of human gait to fuse the stride length information from both feet to get more reliable results. The results of 20 times 20-m walking experiment showed that KUPT is more accurate and reliable than ZUPT, and DFPC could further improve the results of the KUPT method. Another experiment about 91-m indoor walking showed that the proposed localization method could meet the requirement of most IoT applications.

In the future researches, KUPT+DFPC would be applied to IoT applications related to healthcare. In the field of patient or elderly monitoring, KUPT+DFPC could be applied to get higher accuracy on patient localization. When an emergent event (e.g., fall) occurs, the localization information could be helpful to find the patient in time. In addition, gait analysis is another important application of Smart Insole. With the help of KUPT+DFPC method, accuracy of the measured gait parameters, such as stride length and walking velocity etc., could be improved in long-term or out of laboratory assessment.

References

[1] F. Zhang, C. Chen, B. Wang, H.-Q. Lai, Y. Han, and K. J. R. Liu, "Wiball: A time-reversal focusing ball method for decimeter-accuracy indoor tracking," *IEEE Internet Things J.*, vol. 5, no. 5, pp. 4031–4041, Oct. 2018.

[2] A. Brimicombe and C. Li, *Location-Based Services and Geo-Information Engineering*, vol. 21. Chichester, U.K.: Wiley, 2009.

[3] Y. Gu, A. Lo, and I. Niemegeers, "A survey of indoor positioning systems for wireless personal networks," *IEEE Commun. Surveys Tuts.*, vol. 11, no. 1, pp. 13–32, 1st Quart., 2009.

[4] X. Liu, J. Cao, S. Tang, J. Wen, and P. Guo, "Contactless respiration monitoring via off-the-shelf WiFi devices," *IEEE Trans. Mobile Comput.*, vol. 15, no. 10, pp. 2466–2479, Oct. 2016.

[5] F. Adib, H. Mao, Z. Kabelac, D. Katabi, and R. C. Miller, "Smart homes that monitor breathing and heart rate," in *Proc. 33rd Annu. ACM Conf. Human Factors Comput. Syst.*, Seoul, South Korea, 2015, pp. 837–846.

[6] M. G. Puyol, D. Bobkov, P. Robertson, and T. Jost, "Pedestrian simultaneous localization and mapping in multistory buildings using inertial sensors," *IEEE Trans. Intell. Transp. Syst.*, vol. 15, no. 4, pp. 1714–1727, Aug. 2014.

[7] G. Tan, M. Lu, F. Jiang, K. Chen, X. Huang, and J. Wu, "Bumping: A bump-aided inertial navigation method for indoor vehicles using smartphones," *IEEE Trans. Parallel Distrib. Syst.*, vol. 25, no. 7, pp. 1670–1680, Jul. 2014.

[8] G. Oguntala, R. Abd-Alhameed, S. Jones, J. Noras, M. Patwary, and J. Rodriguez, "Indoor location identification technologies for real-time IoT-based applications: An inclusive survey," *Comput. Sci. Rev.*, vol. 30, pp. 55–79, Nov. 2018.

[9] T. C. Michaud, *Human Locomotion: The Conservative Management of Gait-Related Disorders*. Newton, MA, USA: Newton Biomech., 2011.

[10] L. Ojeda and J. Borenstein, "Non-GPS navigation for security personnel and first responders," *J. Navig.*, vol. 60, no. 3, pp. 391–407, 2007.

[11] L. Ojeda and J. Borenstein, "Personal dead-reckoning system for GPS-denied environments," in *Proc. IEEE Int. Workshop Safety Security Rescue Robot. (SSRR)*, Rome, Italy, 2007, pp. 1–6.

[12] E. Foxlin, "Pedestrian tracking with shoe-mounted inertial sensors," *IEEE Comput. Graph. Appl.*, vol. 25, no. 6, pp. 38–46, Dec. 2005.

[13] A. R. Jimenez, F. Seco, C. Prieto, and J. Guevara, "A comparison of pedestrian dead-reckoning algorithms using a low-cost MEMS IMU," in *Proc. IEEE Int. Symp. Intell. Signal Process. (WISP)*, Budapest, Hungary, 2009, pp. 37–42.

[14] G. P. Bailey and R. Harle, "Assessment of foot kinematics during steady state running using a foot-mounted IMU," *Procedia Eng.*, vol. 72, pp. 32–37, Jul. 2014.

[15] F. Dadashi, G. P. Millet, and K. Aminian, "Approaching on-line estimation of swimming instantaneous velocity using a wearable IMU," in *Proc. Int. Symp. 3D Anal. Human Movement*, 2014, pp. 176–179.

[16] N. Lythgo, C. Wilson, and M. Galea, "Basic gait and symmetry measures for primary school-aged children and young adults whilst walking barefoot and with shoes," *Gait Posture*, vol. 30, no. 4, pp. 502–506, 2009.

[17] I. Rishabh, D. Kimber, and J. Adcock, "Indoor localization using controlled ambient sounds," in *Proc. Int. Conf. Indoor Position. Indoor Navig. (IPIN)*, Sydney, NSW, Australia, 2012, pp. 1–10.

[18] H. Bao and W.-C. Wong, "A novel map-based dead-reckoning algorithm for indoor localization," *J. Sensor Actuator Netw.*, vol. 3, no. 1, pp. 44–63, 2014.

[19] K. Wroble, *Performance Analysis of Magnetic Indoor Local Positioning System*. Kalamazoo, MI, USA: Western Michigan Univ., 2015.

[20] E. M. Gorostiza, J. L. Galilea, F. J. Meca, D. S. Monzú, F. E. Zapata, and L. P. Puerto, "Infrared sensor system for mobile-robot positioning in intelligent spaces," *Sensors*, vol. 11, no. 5, pp. 5416–5438, 2011.

[21] E. Brassart, C. Pegard, and M. Mouaddib, "Localization using infrared beacons," *Robotica*, vol. 18, no. 2, pp. 153–161, 2000.

[22] M. Werner, M. Kessel, and C. Marouane, "Indoor positioning using smartphone camera," in *Proc. IEEE Int. Conf. Indoor Position. Indoor Navig. (IPIN)*, Guimaraes, Portugal, 2011, pp. 1–6.

[23] R. Mautz and S. Tilch, "Survey of optical indoor positioning systems," in *Proc. IEEE Int. Conf. Indoor Position. Indoor Navig. (IPIN)*, Guimaraes, Portugal, 2011, pp. 1–7.

[24] M. Kuhn *et al.*, "High accuracy UWB localization in dense indoor environments," in *Proc. IEEE Int. Conf. Ultra Wideband (ICUWB)*, vol. 2. Hannover, Germany, 2008, pp. 129–132.

[25] J.-Y. Lee and R. A. Scholtz, "Ranging in a dense multipath environment using an UWB radio link," *IEEE J. Sel. Areas Commun.*, vol. 20, no. 9, pp. 1677–1683, Dec. 2002.

[26] L. Shangguan, Z. Yang, A. X. Liu, Z. Zhou, and Y. Liu, "STPP: Spatial–temporal phase profiling-based method for relative RFID tag localization," *IEEE/ACM Trans. Netw.*, vol. 25, no. 1, pp. 596–609, Feb. 2017.

[27] D. K. Barton, *Radar System Analysis and Modeling*, vol. 1. Boston, MA, USA: Artech House, 2004.

[28] C. Fuchs, N. Aschenbruck, P. Martini, and M. Wieneke, "Indoor tracking for mission critical scenarios: A survey," *Pervasive Mobile Comput.*, vol. 7, no. 1, pp. 1–15, 2011.

[29] O. J. Woodman, "An introduction to inertial navigation," Comput. Lab., Univ. Cambridge, Cambridge, U.K., Rep. UCAM-CL-TR-696, 2007.

[30] K.-C. Lan and W.-Y. Shih, "Using smart-phones and floor plans for indoor location tracking—Withdrawn," *IEEE Trans. Human–Mach. Syst.*, vol. 44, no. 2, pp. 211–221, Apr. 2014.

[31] D. Gusenbauer, C. Isert, and J. Krösche, "Self-contained indoor positioning on off-the-shelf mobile devices," in *Proc. Int. Conf. Indoor Position. Indoor Navig. (IPIN)*, Zürich, Switzerland, 2010, pp. 1–9.

[32] J. A. B. Link, P. Smith, N. Viol, and K. Wehrle, "FootPath: Accurate map-based indoor navigation using smartphones," in *Proc. IEEE Int. Conf. Indoor Position. Indoor Navig. (IPIN)*, Guimaraes, Portugal, 2011, pp. 1–8.
[33] B. Zhou, Q. Li, Q. Mao, W. Tu, and X. Zhang, "Activity sequence-based indoor pedestrian localization using smartphones," *IEEE Trans. Human–Mach. Syst.*, vol. 45, no. 5, pp. 562–574, Oct. 2015.
[34] K.-C. Lan and W.-Y. Shih, "On calibrating the sensor errors of a PDR-based indoor localization system," *Sensors*, vol. 13, no. 4, pp. 4781–4810, 2013.
[35] I. Skog, P. Handel, J.-O. Nilsson, and J. Rantakokko, "Zero-velocity detection—An algorithm evaluation," *IEEE Trans. Biomed. Eng.*, vol. 57, no. 11, pp. 2657–2666, Nov. 2010.
[36] J. Ruppelt, N. Kronenwett, G. Scholz, and G. F. Trommer, "High-precision and robust indoor localization based on foot-mounted inertial sensors," in *Proc. IEEE/ION Position Location Navig. Symp. (PLANS)*, Savannah, GA, USA, 2016, pp. 67–75.
[37] A. Norrdine, Z. Kasmi, and J. Blankenbach, "Step detection for ZUPT-aided inertial pedestrian navigation system using foot-mounted permanent magnet," *IEEE Sens. J.*, vol. 16, no. 17, pp. 6766–6773, Sep. 2016.
[38] M. Romanovas *et al.*, "A study on indoor pedestrian localization algorithms with foot-mounted sensors," in *Proc. Int. Conf. Indoor Position. Indoor Navig. (IPIN)*, Sydney, NSW, Australia, 2012, pp. 1–10.
[39] Q. Fan *et al.*, "An optimal enhanced Kalman filter for a ZUPT-aided pedestrian positioning coupling model," *Sensors*, vol. 18, no. 5, p. 1404, 2018.
[40] C. Fischer, P. T. Sukumar, and M. Hazas, "Tutorial: Implementing a pedestrian tracker using inertial sensors," *IEEE Pervasive Comput.*, vol. 12, no. 2, pp. 17–27, Apr./Jun. 2013.
[41] I. Skog, J.-O. Nilsson, and P. Händel, "Evaluation of zero-velocity detectors for foot-mounted inertial navigation systems," in *Proc. Int. Conf. Indoor Position. Indoor Navig. (IPIN)*, Zürich, Switzerland, 2010, pp. 1–6.
[42] P. Strömbäck *et al.*, "Foot-mounted inertial navigation and cooperative sensor fusion for indoor positioning," in *Proc. ION Int. Techn. Meeting (ITM)*, 2010, pp. 89–98.
[43] M. Romanovas *et al.*, "Pedestrian indoor localization using foot mounted inertial sensors in combination with a magnetometer, a barometer and RFID," in *Progress in Location-Based Services*. Heidelberg, Germany: Springer, 2013, pp. 151–172.
[44] A. R. J. Ruiz, F. S. Granja, J. C. P. Honorato, and J. I. G. Rosas, "Pedestrian indoor navigation by aiding a foot-mounted IMU with RFID signal strength measurements," in *Proc. Int. Conf. Indoor Position. Indoor Navig. (IPIN)*, Zürich, Switzerland, 2010, pp. 1–7.
[45] A. R. J. Ruiz, F. S. Granja, J. C. P. Honorato, and J. I. G. Rosas, "Accurate pedestrian indoor navigation by tightly coupling foot-mounted IMU and RFID measurements," *IEEE Trans. Instrum. Meas.*, vol. 61, no. 1, pp. 178–189, Jan. 2012.
[46] H. Ju, M. S. Lee, S. Y. Park, J. W. Song, and C. G. Park, "A pedestrian dead-reckoning system that considers the heel-strike and toe-off phases when using a foot-mounted IMU," *Meas. Sci. Technol.*, vol. 27, no. 1, 2015, Art. no. 015702.
[47] D. Chen, Y. Cai, and M.-C. Huang, "Customizable pressure sensor array: Design and evaluation," *IEEE Sensors J.*, vol. 18, no. 15, pp. 6337–6344, Aug. 2018.
[48] X. Zhang, Z. Yang, T. Chen, D. Chen, and M.-C. Huang, "Cooperative sensing and wearable computing for sequential hand gesture recognition," *IEEE Sensors J.*, to be published.
[49] Ö. Bebek *et al.*, "Personal navigation via high-resolution gait-corrected inertial measurement units," *IEEE Trans. Instrum. Meas.*, vol. 59, no. 11, pp. 3018–3027, Nov. 2010.
[50] A. Gabell and U. S. L. Nayak, "The effect of age on variability in gait," *J. Gerontol.*, vol. 39, no. 6, pp. 662–666, 1984.
[51] D. Chen, J. Chen, H. Jiang, and M.-C. Huang, "Risk factors identification for work-related musculoskeletal disorders with wearable and connected gait analytics system," in *Proc. IEEE/ACM Int. Conf. Connected Health Appl. Syst. Eng. Technol. (CHASE)*, Philadelphia, PA, USA, 2017, pp. 330–339.
[52] D. Chen, Y. Cai, J. Cui, J. Chen, H. Jiang, and M.-C. Huang, "Risk factors identification and visualization for work-related musculoskeletal disorders with wearable and connected gait analytics system and kinect skeleton models," *Smart Health*, vols. 7–8, pp. 60–77, Jun. 2018.

Diliang Chen is currently pursuing the Ph.D. degree in computer engineering at Case Western Reserve University, Cleveland, OH, USA.

His current research interests include exploring novel sensing and computing technologies to build Internet of Things systems for healthcare and worker safety.

Huiyi Cao is currently pursuing the M.S. degree in computer science at the Electrical Engineering and Computer Science Department, Case Western Reserve University, Cleveland, OH, USA.

Her current research interests include mobile health software development and data analysis.

Huan Chen is currently pursuing the Ph.D. degree in computer engineering at Case Western Reserve University, Cleveland, OH, USA.

His current research interests include wireless communication, software development, and security.

Zetao Zhu is currently pursuing the master's degree in computer engineering at Case Western Reserve University, Cleveland, OH, USA.

His current research interests include developing healthcare application on Android and HoloLens platforms.

Xiaoye Qian received the M.S. degree from the Electrical Engineering and Computer Science Department, Case Western Reserve University, Cleveland, OH, USA.

His current research interests include wearable systems for human health care and data analytics using machine learning with Internet of Things systems.

Wenyao Xu (M'13) received the B.S. and M.S. degrees (Hons.) from Zhejiang University, Hangzhou, China, in 2006 and 2008, respectively, and the Ph.D. degree from the University of California at Los Angeles, Los Angeles, CA, USA, in 2013.

He is an Associate Professor with the Computer Science and Engineering Department, State University of New York at Buffalo, Buffalo, NY, USA. He has intensively collaborated with many industrial companies over the past years. He has authored or coauthored over 160 research papers, coauthored 2 books, and has invented 6 international and U.S. patents. His current research interests include smart health, Internet of Things, and emerging biometrics.

Dr. Xu was a recipient of six Best Paper Awards in his research fields. He has served on the Technical Program Committee of numerous international conferences in the field of smart health, mobile computing, and Internet of Things, and was the TPC Co-Chair of IEEE BSN 2018.

Ming-Chun Huang (M'14) received the Ph.D. degree in computer science from the University of California at Los Angeles, Los Angeles, CA, USA.

He is an Assistant Professor with the Electrical Engineering and Computer Science Department, Case Western Reserve University, Cleveland, OH, USA. He aims to create novel devices and analytical algorithms that offer enhanced functionality and performance over conventional tools and technologies in terms of portability, rapid analysis time, and user-friendly operation. His research and education vision is to explore and share creative solutions to address current and emerging challenges facing our society in the 21st Century, including adapting wearables as biomarkers for improving workplace and community safety and health services. For the nature of richness and high impact of the topics involved, his research will immediately generate a plethora of new knowledge in aspects ranging from innovative sensing technology, advanced data analytics methodology, and optimized clinical decision-making and risk assessment.